Dalton Transactions

Accepted Manuscript

This article can be cited before page numbers have been issued, to do this please use: M. A. Iqbal, L. Sun, A. M. LaChance, H. Ding and M. Fedel, *Dalton Trans.*, 2019, DOI: 10.1039/C9DT01773A.

This is an Accepted Manuscript, which has been through the Royal Society of Chemistry peer review process and has been accepted for publication.

Accepted Manuscripts are published online shortly after acceptance, before technical editing, formatting and proof reading. Using this free service, authors can make their results available to the community, in citable form, before we publish the edited article. We will replace this Accepted Manuscript with the edited and formatted Advance Article as soon as it is available.

You can find more information about Accepted Manuscripts in the author guidelines.

Please note that technical editing may introduce minor changes to the text and/or graphics, which may alter content. The journal's standard Terms & Conditions and the ethical guidelines, outlined in our author and reviewer resource centre, still apply. In no event shall the Royal Society of Chemistry be held responsible for any errors or omissions in this Accepted Manuscript or any consequences arising from the use of any information it contains.

ROYAL SOCIETY OF CHEMISTRY

rsc.li/dalton

View Article Online
DOI: 10.1039/C9DT01773A

In situ Growth of CaAl-NO_3^--Layered Double Hydroxide Directly on Aluminum Alloy for Corrosion Resistance.

Muhammad Ahsan Iqbal[1,2*], Luyi Sun[2*], Anna Marie LaChance[2], Hao Ding[2], Michele Fedel[1]

[1)]Department of Industrial Engineering, University of Trento, via Sommarive 9, Povo (TN), Italy

[2)]Polymer Program, Institute of Materials Science and Department of Chemical and Biomolecular Engineering, University of Connecticut, Storrs, CT 06269, USA

Corresponding email: Luyi Sun (luyi.sun@uconn.edu)

Muhammad Ahsan Iqbal (muhammadahsan.iqbal@unitn.it)

Abstract

In this study, a calcium-aluminum-layered double hydroxide (CaAl-LDH) thin film was grown on AA6082 aluminum alloy, for the very first time, by using a facile in situ growth method in an effort to investigate the CaAl-LDH structural geometry and corresponding corrosion resistance properties. The structure and surface morphologies of the CaAl-LDH thin film were studied through scanning electron microscopy (SEM) equipped with an EDS detector, transmission electron microscopy (TEM), X-ray diffractometer (XRD), Fourier transform infrared spectrometer (FT-IR), while electron impendence spectra (EIS) and potentiodynamic curves were collected to understand the LDH anticorrosion behavior. The findings demonstrated that thin, well-developed CaAl-LDH coatings with different surface morphologies can be prepared with eminent corrosion resistance properties. Specifically, the CaAl-LDH thin film synthesized at 140 ˚C-24 h synthetic condition showed a large impedance modulus of 7.3 Ω cm^2 at 0.01 Hz ($|Z|_f$ = 0.01 Hz), along with a low corrosion current density (I_{corr}) of 0.0007 μA cm^{-2}, while a vertically-orientated rod like structure with uniform surface morphology was observed.

Keywords: in situ growth, CaAl-LDH thin film, aluminum alloy, corrosion resistance.

View Article Online
DOI: 10.1039/C9DT01773A

1. Introduction

Aluminum and its alloys are applied in numerous applications due to their natural abundance, high strength-to-weight ratio, and relatively low cost. However, due to the high reactivity of aluminum alloys, they are highly susceptible to localized corrosion on exposure with a neutral corrosive environment, and to uniform corrosion on contact with an acidic or alkaline medium, which hinders their service durability [1, 3]. For this reason, various surface functionalization treatments have been attempted to protect the aluminum surface, including vapor deposition[4], magnetron sputtering [5-6], electroplating [7], Sol-gel coatings [8-9], anodic oxidation [10-11], chemical conversion coatings [12-13] and so on.

In recent years, layered double hydroxide chemical conversion films have also aroused widespread attention as protective anti-corrosion films for metallic substrates due to LDH's unique characteristics, including their eco-friendly nature, multifunctional characteristics, availability of a wide range of anionic and cationic combinations, self-healing and ion-exchange capabilities, high surface area, cost-effectiveness and good adhesion with substrates. The LDHs, members of a two-dimensional brucite structure-family of synthetic anionic clays, could be expressed by the general formula $[M^{2+}_{1-x}M^{3+}_{x}.\ x(OH)_2]A^{n-}_{x/n}\cdot mH_2O]$, where M^{2+} and M^{3+} are the divalent and trivalent cations respectively, while A^{-1} are the anions present inside the LDH interlayers. The LDH structure is formed when some of the divalent cations are substituted by the trivalent cations, while the intercalation of anions stabilizes the residual positive charge, thus a brucite-like layered structure is obtained [12-15]. Generally, two primary synthetic approaches are used to develop layered double hydroxides; the physical deposition and the in-situ growth method. In the former technique, the LDH is developed by a hydrothermal growth method and further deposition on the substrate is separately made via different approaches. Meanwhile, the in-situ growth method is considered more effective; here, an LDH film is grown directly on the substrate, which has shown better adhesion properties due to strong chemical bonding between the two phases and thus helps to prolong the corrosion resistance properties of LDHs [16-17].

Previously, different combinations of divalent cations (X= Mg^{+2}, $Zn^{+2,}$ Li^{+2}) have been investigated to develop layered double hydroxide corrosion-protective films on aluminum substrates by the in-situ growth method, where the aluminum substrate act as both the source of the trivalent cation and also the support for the reaction [12-13, 18-19]. In terms of the ion-exchange equilibrium constant, charge compensating LDH anions have the following

View Article Online
DOI: 10.1039/C9DT01773A

progression: CO_3^- > SO_4^-> OH^-> F^-> Cl^-> Br^-> NO_3^- [20]. Therefore, NO_3^{1-}-intercalated LDH could be a reasonable choice where anion exchange with the corrosive species (Cl^-, F^-, Br^-, SO_4^-) is a solution to enhance the anticorrosive properties by strongly holding these anions inside the LDH interlayer's, while NO_3^- ions also facilitate the reaction kinetics to further modify the LDH chemistry with different corrosion inhibitors to develop a more compact protective LDH structure [21]. There are a number of reports where CaAl-LDH is investigated in different applications of biomedical science, environmental science and catalysis [22-24]; however, there has not been any report on in-situ growth of CaAl-LDH films on metallic substrates and the characterization of their corrosion resistance properties.

CaAl-LDH belongs to the hydrocalumite subgroup of hydrotalcites [25] and is heptahedrally coordinated with the aluminum ions, instead of octahedral coordination, due to relatively large size of Ca^{2+} ions compared to the Mg^{2+} and Zn^{2+} cations (thoroughly-investigated LDH cations[26], whilst the seventh coordination site is occupied by a hydroxyl group and/or with compensating anions [27]. Although it is difficult to obtain a pure, thermodynamically-uniform CaAl-LDH phase—different secondary phases can also be favored during the synthesis—our intentions, here, are to elucidate the development of CaAl-LDH as a protective thin film on the aluminum surface and their role as a corrosion-protective film.

Herein, we synthesized CaAl-NO_3-LDH thin films on AA6082 aluminum alloy at different synthetic conditions to investigate their structural properties and corrosion resistance. The structural growth of CaAl-LDH can be controlled by extending the crystallization time from 12 to 72 h at the 140˚C reaction temperature (adjusted based on our preliminary results) in an alkaline solution of pH 10. The crystallization time was found to promote the LDH structural growth and a range of CaAl-LDHs coatings exhibiting different structural geometries with unique morphologies and improved corrosion resistance properties were obtained.

2. Materials

The AA6082 ingot was purchased from Metal Center (Italy) with a chemical composition of (0.70 - 1.30) percent Silicon, (0.40-1.00) percent manganese, (0.60 - 1.20) percent magnesium, (0.50) percent iron, (0.10 percent) copper, with a balanced percentage of aluminum. $CaNO_3.4H_2O$ (≥98%) and NaOH (≥98%) were purchased from Sigma Aldrich.

3. Synthesis of CaAl-NO_3-layered double hydroxide

In our approach, the CaAl-LDH thin films were grown on AA6082 alloy by a facile one-step method at a temperature of 140˚C for different crystallization times, i.e. 12 h, 18h, 24h, and 72 h.

View Article Online
DOI: 10.1039/C9DT01773A

The aluminum alloy was initially ground with SiC of 1200, 1600, 4000 grit paper and degreased in 0.1 M NaOH for one minute and further ultrasonically treated in ethanol solution for ten minutes. 70 mL of 0.02M $CaNO_3.4H_2O$ solution was prepared and purged with nitrogen gas to remove absorbed gases and transferred into a 100mL Teflon-lined autoclave. The pH of the solution was adjusted to 10 with the dropwise addition of NaOH. The pretreated aluminum substrates (3.14 cm^2) which act as a source of Al^{3+} were placed in the above solution and were treated in an oven at 140˚C temperature for 12, 18, 24 and 72h crystallization time for in-situ growth CaAl-LDH on the aluminum alloy. After experiment completion, the coated specimens were washed with deionized water and were dried with nitrogen gas.

4. Characterization

The surface morphologies and structural geometries of the CaAl-LDH thin films were investigated by scanning electron microscopy (JEOL JSM-6330F) equipped with an EDS detector (Thermo Noran System Six). For transmission electron microscopy images, the sample was dispersed in ethanol using ultrasonication and deposited on a 400-mesh copper grid, and the images were recorded under an FEI Talos F200X scanning transmission electron microscope. The X-ray diffractometer (Bragg – Brentano fixed sample theta-theta geometry) with a LynxEye linear detector, copper K-α emission source, λ=1.5406 $Å^{-1}$) was used to characterize the microstructure at 10 mA and 30 kV conditions, while FTIR spectra (NICOLET MAGNA 560) were recorded to analyze surface functional groups and the chemical bonding of the samples in ATR mode. The potentiodynamic curves and EIS were collected through CHI600 (CH Instruments, Inc) with a traditional three-electrode system with Ag/AgCl (+207 mV vs. SHE) and platinum foil as the reference and counter electrode respectively, with the as-prepared CaAl-LDH (3.14 cm^2 exposed area) as the working electrode. The Tafel measurement was performed at a scan rate of 2 mV/s in the potential region of ±500 mV versus OCP. EIS measurements were acquired from 100 kHz down to 10 mHz, using a 5 mV (rms) amplitude perturbation. All potentiostatic and EIS measurements were made in 0.1M NaCl solution at room temperature with delay period of 30 minute to stable the electrochemical system.

.

5. Results and Discussion

Figure 1(a-d) shows the SEM images of CaAl-LDH microstructure. It can be seen that with the increase of crystallization time from 12 to 24 h, the CaAl-LDH structure becomes more regular and the crystallite size grows bigger until 140˚C-24h, while for 140˚C-72h the cones were found

View Article Online
DOI: 10.1039/C9DT01773A

to have transformed into compact nest-like microstructures and the intermixed uniform curvy structure can be visualized. The difference in morphology of CaAl-LDH can be related to the extended crystallization time which can be attributed to the variation in Ca/Al weight ratio (examined by EDS analysis) and also due to the variation in absorption of NO_3^{1-} anions inside LDH interlayers (confirmed by XRD analysis). The surface of the LDH matrix was covered with horizontally- and vertically-aligned nano-flake arrays, mainly composed of Ca, Al, N, and O. The Ca/Al weight % ratio was found to vary from 1:7 at (140˚C-12h) to 1:5 at (140˚C-72h) and around 1:4 for 72 h specimens. The high Ca/Al ratio and higher NO_3^{1-} ion intercalation caused both an increased growth rate of CaAl-LDH and also an increase of nucleation density of NO_3^{1-} anions, which remarkably influenced the structural geometry of CaAl-LDH.

The layered structure of CaAl-LDH, synthesized at 140 ˚C-24h, could be observed under TEM, as shown in Figure 2. During sample dispersion, the ultrasonication power might destroy the cone-like structure of most crystals, yet some triangular features remained as shown by the arrow in Figure 2a. The corresponding TEM diffraction pattern (Figure 2b) gave rings with bright spots, suggesting that the sample is polycrystalline and has some preferred orientations. The two rings with the smallest radii indicate an interplanar spacing of 3.1 and 2.8 Å, respectively, which accord with the two strongest peaks in the XRD pattern (Figure 3). The layered structures of CaAl-LDH can be seen at higher magnification in Figure 2c.

The crystal structure and phase identification of CaAl-LDH were confirmed with XRD analysis as shown in Figure 3. The XRD pattern of the CaAl-LDH is similar to those previously reported by Szabados, Márton, et al for co-precipitated CaAl-LDHs [28]. The intercalation of NO_3^{1-} anions inside LDH interlayers is confirmed by the (001) reflection peaks at the low 2θ value of 12.4º [28], which sharpened with respect to extended crystallization time indicating the relatively high crystallinity. The peak broadening is generally attributed to crystallite size effects and non-uniform broadening of anisotropic crystallites. The interlayer region mainly contains the hydroxyl groups and nitrate ions to balance the positive charge layers, while the peak at (001) planes of CaAl-LDH was used to measure the basal spacing's of developed films by using Bragg's equation. The interlayer distance of CaAl-LDH at "001" lies around 0.8nm, which on prolonged crystallization time contract slightly, due to different NO_3^{1-} anions and hydroxyl group orientation inside the interlayers. The obtained value of basal spacing corresponds to the sum of nitrate anions and hydroxyl groups, which is in agreement with the literature data [29]. The cell

View Article Online
DOI: 10.1039/C9DT01773A

parameter "c" found to elevate possibly due to the different size, strength and bonding orientation of the hydroxyl group and nitrate anions inside the brucite-like structure, with the effect of the increasing reaction treatment time. Besides the CaAl-LDH characteristics peaks, few other peaks were also found, which correspond to the formation of $Ca(OH)_2$ and $Al(OH)_3$. It was previously reported that due to exothermic dissolution, $Ca(OH)_2$ and $Al(OH)_3$ are also formed, which did not convert into an LDH structure. However, their concentration was found to decrease with extended crystallization time, and some $Ca(OH)_2$ is also transformed into TCA (Tricalcium-aluminate) [28]. The XRD patterns showed that the overall LDH characteristic structure remained well-preserved during thermal treatment from the 12 to 72 h crystallization time period; however, this extended time period caused the contraction of basal spacing, which is well consistent with the results of the literature study [12, 13, 30]. The interlayer thickness at d_{001}, full width half maximum and corresponding crystallite sizes (calculate by Scherrer formula) are listed in Table 1.

Table 1. Cell parameters of the CaAl-LDH structure synthesized at 140 ˚C for different reaction time.

	12 h	18 h	24 h	72 h
d_{001} (nm)	0.832	0.821	0.818	0.820
FWHM	0.413	0.317	0.231	0.238
Crystallite size (nm)	22.3	29.0	39.3	38.4

The FTIR spectra of all the obtained CaAl-LDHs are shown in Figure 4. The main bands at wavenumber 1365-1389 cm^{-1} and 3450 cm^{-1} are assigned to the presence of the NO_3^{1-} group, and O–H vibration mode of the hydroxyl group and water molecules respectively [31, 32]. A small bending around 1627cm^{-1} corresponds to the bending vibration of water molecules while in the low-frequency range and the band spectra at 532, 785 cm^{-1} corresponds to M-O vibration bonds [33, 34]. Due to carbon dioxide contamination from the air during the synthesis of LDH, the broadness of the nitrate band can be attributed to the overlapping of nitrate and carbonate ions from 1360 to 1370 cm^{-1}, especially in case of the 140˚C-72h specimen; this peak is bit-shifted, probably due to the presence of carbonate groups.

View Article Online
DOI: 10.1039/C9DT01773A

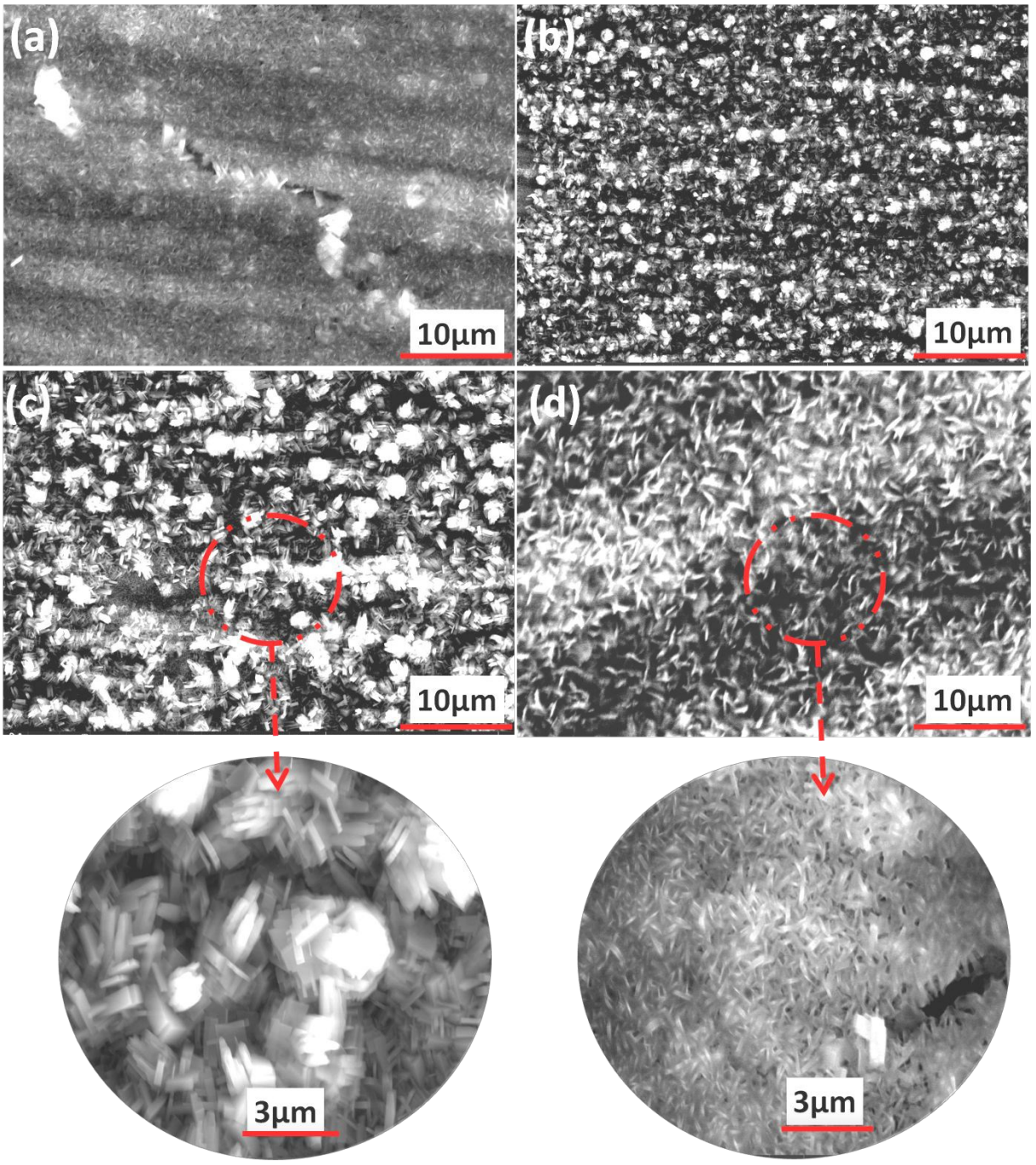

Figure 1. SEM images of the CaAl-LDH films synthesized at various conditions: (a) 140 ˚C-12 h, (b)140 ˚C-18 h, (c) 140 ˚C-24 h, and (d)140 ˚C-72 h.

View Article Online
DOI: 10.1039/C9DT01773A

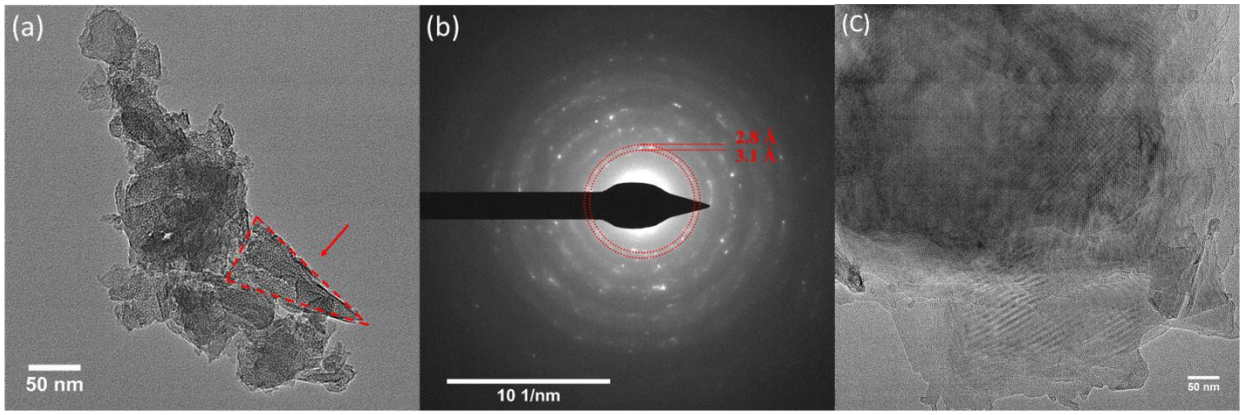

Figure 2. (a) TEM image of the CaAl-LDH film synthesized at 140 ˚C-24h, (b) corresponding diffraction pattern, (c) interplaner spacing lines of layered structure in the high-resolution image.

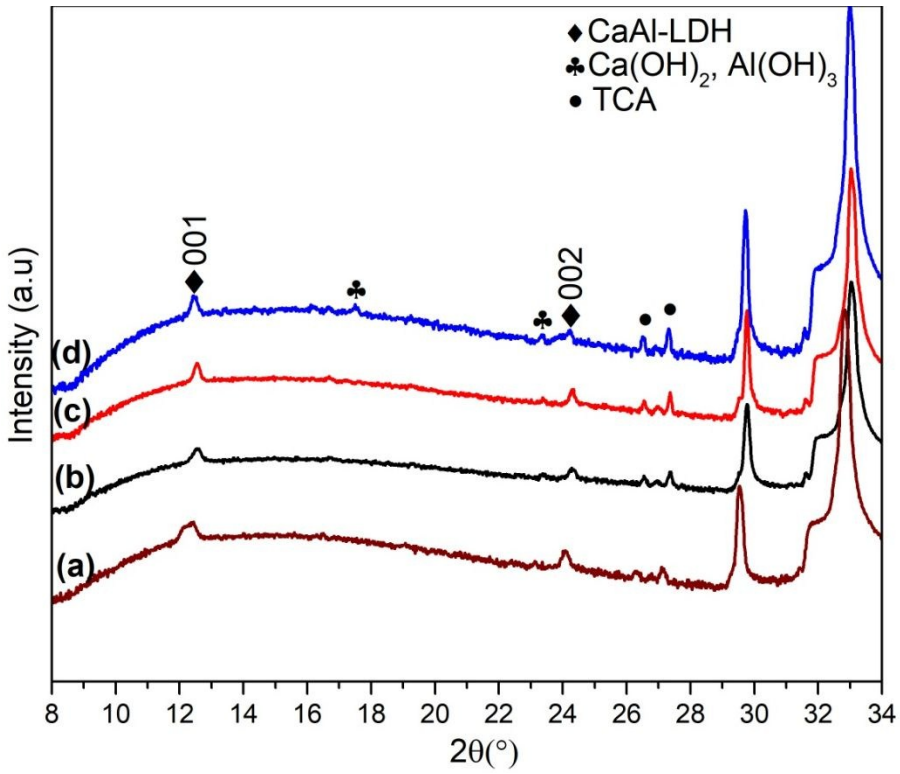

Figure 3. XRD patterns of CaAl-LDH film samples synthesized on AA6082: (a) 140 ˚C-12 h, (b) 140 ˚C-18 h, (c) 140 ˚C-24 h, and (d) 140 ˚C-72 h.

View Article Online
DOI: 10.1039/C9DT01773A

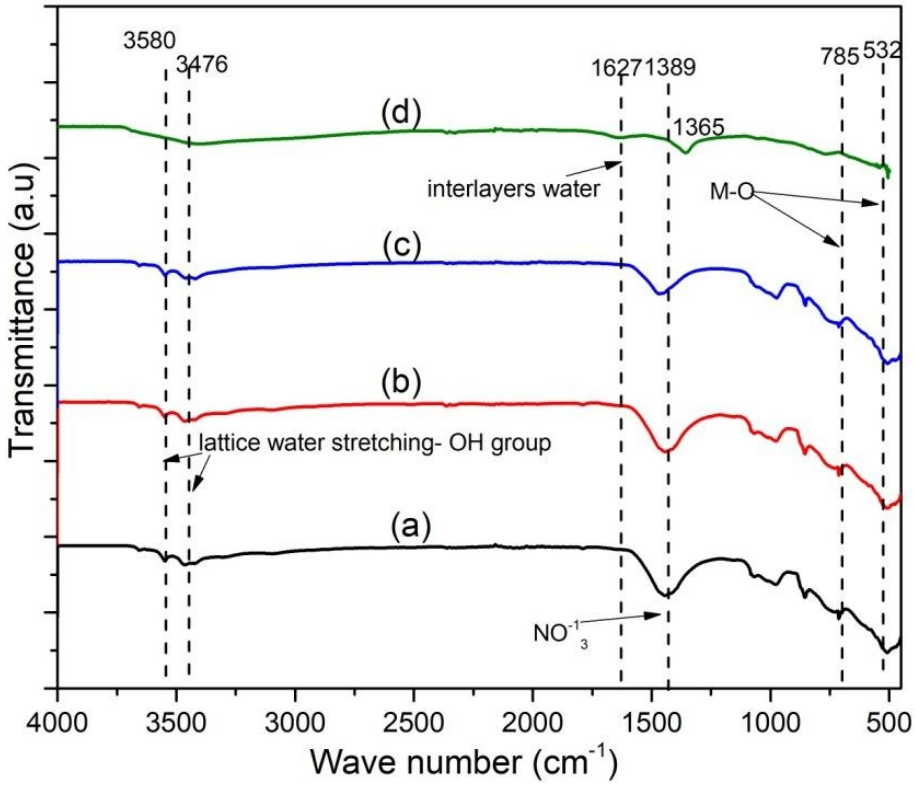

Figure 4. FTIR spectra of CaAl-LDH synthesized at 140 ˚C for different crystallization time: (a) 12 h, (b) 18 h, (c) 24 h, and (d) 72 h.

To understand the corrosion resistance properties of CaAl-LDH, the Tafel polarization curves were employed (Figure 6), which can be an effective way to understand the corrosion current density and corrosion current potential. Notice that the bare AA6082 showed an almost passive current at about 10^{-6} A cm^{-2} for anodic overpotential in the range of 250-300 mV. CaAl-LDH coated substrates did not show any more of a clear passive transient. However, an increase in corrosion potential is observed for all the investigated samples, regardless of the crystallization conditions. The LDH coatings derived from deposition times of 12 and 18 h seem not to provide any significant improvement in terms of cathodic or anodic current density reduction. On the other hand, the CaAl-LDH coated samples showed a noticeable reduction of both anodic and cathodic corrosion current compared to the bare substrate. In particular, the coating derived from deposition time of 24 h demonstrated a decrease in anodic current density of about 3-4 orders of magnitude. Notice that the reduction in current density is not proportional to the increase in film thickness, as one can observe from Figure 5(b). This finding will be discussed throughout the paper. The film thickness (barrier effect), up to an extent, can also be a responsible factor to reduced anodic and cathodic current densities and therefore is expected to impart an influential

View Article Online
DOI: 10.1039/C9DT01773A

impact on the corrosion resistance properties. Figure 5(a) depicts the cross-sectional optical analysis of CaAl-LDH of the 140˚C-24h specimen. The significant reduction of I_{corr} and the more positive corrosion potential of CaAl-LDH specimens is attributed to the reduction of anodic and cathodic sites on the CaAl-LDH surface. As reported in our earlier works, the extended crystallization time can result in the more compact layered-double architecture and such behavior can also reorient the LDH as a strong barrier against the corrosive solutions [12, 13], which is well-consistent with the current study, where extended crystallization times facilitate to improve the overall CaAl-LDH corrosion resistance properties up to an extent. The increase in corrosion resistance properties of the aluminum can be due to the following factors: (1) the anion exchangeability of the CaAl-LDH film with the Cl^{1-} ions, (2) the strong barrier properties of CaAl-LDH attributed to strong LDH adhesion with the substrate and its compact nest-like structure. The calculated corrosion current density and corrosion potential of developed specimens are listed in Table 2. Figure 5(b) shows the impact of extended crystallization time on the film thickness, which increased from 9.5 to almost 12µm with the increase of crystallization time from 12 h to 72 h.

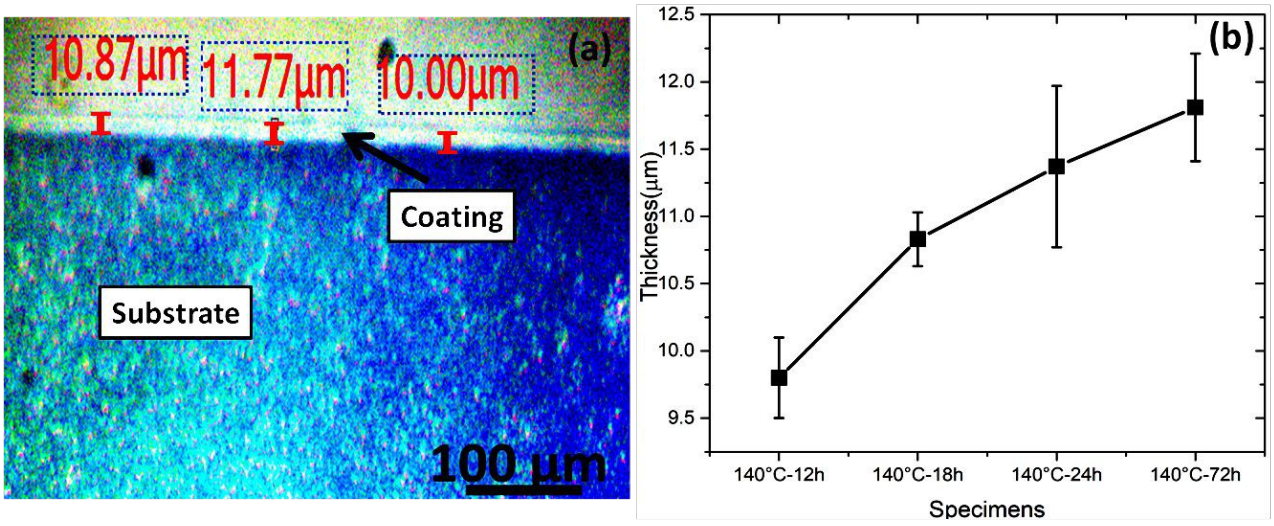

Figure 5. (a) Cross-sectional optical image of the CaAl LDH film coated on AA6082 alloy at 140 ˚C-24 h and (b) measured thickness from cross-sectional analysis of the as-prepared coatings.

View Article Online
DOI: 10.1039/C9DT01773A

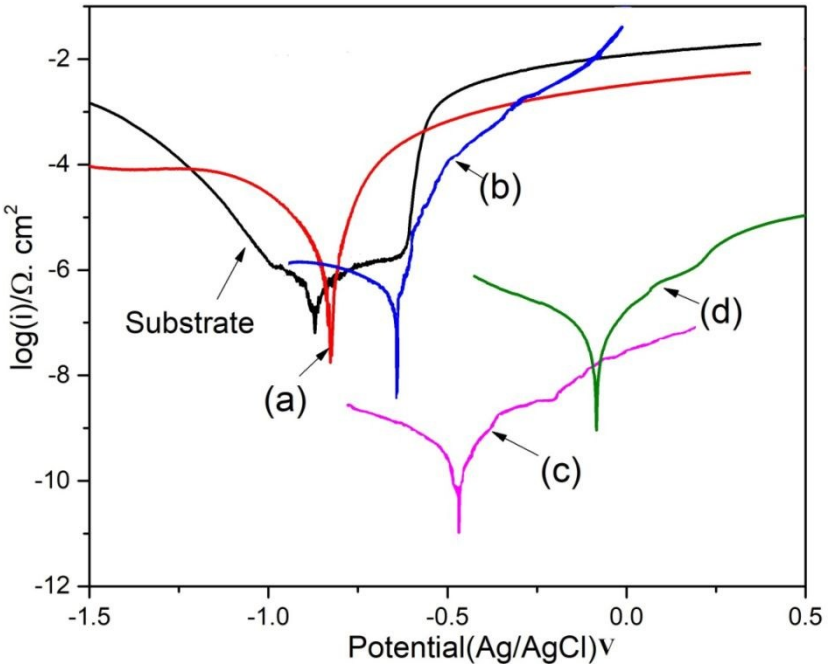

Figure 6. Polarization curves of the bare AA6082 and the CaAl-LDH coated AA6082 specimens in 0.1 M NaCl aqueous solution: (a) 140 ˚C-12 h, (b) 140 ˚C-18 h, (c) 140 ˚C-24 h, and (d) 140 ˚C-72 h.

Table 2. Electrochemical parameters estimated from the polarization data in Figure 5.

	Corrosion current density ($\mu A/cm^2$)	Potential (Ag/AgCl) V
AA6082	0.7581	-0.879
140 ˚C-12 h	0.6752	-0.831
140 ˚C-18 h	0.3312	-0.649
140 ˚C-24 h	0.0007	-0.473
140 ˚C-72 h	0.0623	-0.087

In order to further evaluate the electrochemical behavior of CaAl-LDH thins films, EIS characterization was carried out in 0.1M NaCl electrolyte as shown in Figure 7(a-b). The reason for using a relatively mild electrolyte (0.1M NaCl) relies on the intention to better highlight the small differences among the studied samples, considering the small variation of crystallization time and growth behavior on the corrosion-resistance properties. EIS results of bare AA6082 substrate showed two zones, one capacitive zone in the middle frequency range (10^3-10^0 Hz) and one resistance zone in the low-frequency region (below 10^0 Hz). The low-frequency impedance ($|Z|_{00.1}$) for the bare sample is about 4.5×10^4 Ω cm^2. The impedance modulus at a low frequency, such as $|Z|_{00.1}$ can be used to compare the corrosion-resistant capability of coatings [35]. It can be observed from the Bode plots that the LDH-coated samples exhibit higher impedance in the low-

View Article Online
DOI: 10.1039/C9DT01773A

frequency domain (0.1-0.01 Hz) compared with the bare aluminum alloy sample. It is also worthy to note that the impedance modulus of CaAl-LDH at the optimum synthetic conditions (140˚C-24h) have more than two orders of magnitude higher than that of the Al substrate at 0.01 Hz. The strong shift of the impedance in the middle-high frequency range is attributed to the presence of the coating. The presence/absence of the shift in impedance in this range provides information related to the real presence of a dielectric coating on the surface of the metal. The samples developed at 140˚C-24 and 72h have demonstrated an almost capacitive behavior in the middle-high frequency range (Figure 7(a)), thus suggesting the presence of a dielectric LDH coating, and their deviation reflects the LDH surface roughness and degree of homogeneity [36, 37]. The other developed coatings at the lower crystallization times have shown much lower values of electrochemical impedance in the investigated frequency range (Figure 7(a)). The specimens at 140˚C-12 h and 18h have shown two partially overlapped peaks in the phase angle spectrum with a slight increase in impedance which likely indicates a nonuniform and defective surface and, therefore, only slight protection. According to the relevant increase in thickness obtained by increasing the treatment time, the electrochemical response of the investigated samples remarkably differs from one sample to another. The presence of inhomogeneities and defects, occurred during the synthesis of the coatings, furtherly exacerbate the differences among the EIS spectra of the samples. Considering the Figure 7(b), the EIS response suggests that only the coatings at high crystallization time have shown the capacitive response in the middle-high frequency range, with high impedance values which describe well-protective CaAl-LDH thin films. The samples at 140˚C-24 h have shown a relevant increase of the low-frequency impedance (from 10^4 to 10^7 Ωcm^2) compared to the bare aluminum sample. These coatings seem to be protective, thanks to the relevant increase in impedance, but they are likely to be partially porous, permeable and/or defective as they do not show a clear capacitive behavior.

Figure 8(a) shows the XRD spectra of CaAl-LDH thin film developed at 140˚C-24h before and after immersion in 0.1M NaCl solution for 4 and 7 days. It can be seen that the (001) characteristic peak of CaAl-LDH is shifted towards a higher degree after immersion in chloride solution, which indicates the strong intercalation of chloride anions in the LDH galleries, indicative of anion-exchange of NO_3^{1-} with the Cl^{1-}. It is well-consistent with a number of other reports that describe the chloride exchange behavior with the nitrate ions, due to the higher binding energy of chloride ions compared to the nitrate ions [38]. When compared to a 7-day

View Article Online
DOI: 10.1039/C9DT01773A

immersion, the shift towards a higher degree is more evident in a 4-day-immersion (due to a large amount of chloride uptake from the solution after 4 days) and the concentration of chlorides on the solution decreases (which further slows down the diffusion rate); after 7 days, a negligible shift was observed in the diffraction peak of CaAl-LDH. Figure 8(b) depicts the stability of the impedance modulus and its evolution with the immersion time. The specimen (140˚C-24h) were immersed in 0.1M NaCl solution for 4 and 7 days and after that impedance plots were collected to understand the evolution of impedance on contact with the corrosive solution. The value of decrease is comparatively higher in the low-frequency range ($|Z|_{00.1}$), and after 7 days of immersion, an almost one order magnitude decrease in the low-frequency range was observed. This evolution of decrease in impedance spectra can be explained due to following: with the passage of time, the electrolyte filled the porous structure of LDH, and as time elapsed, the chloride solution moved through the pores and defects which decrease the film resistance. Figure 9 shows the cross-sectional image of CaAl-LDH(140˚C-24h) after a 7-day immersion in 0.1M NaCl solution. As it can be seen, on contact with the NaCl solution, the CaAl-LDH film remained intact with strong contact to the substrate, and a bit compactness of the structure can also be observed with almost the same original film thickness. Insets are the surface camera images of the thin film before and after immersion in 0.1M NaCl solution.

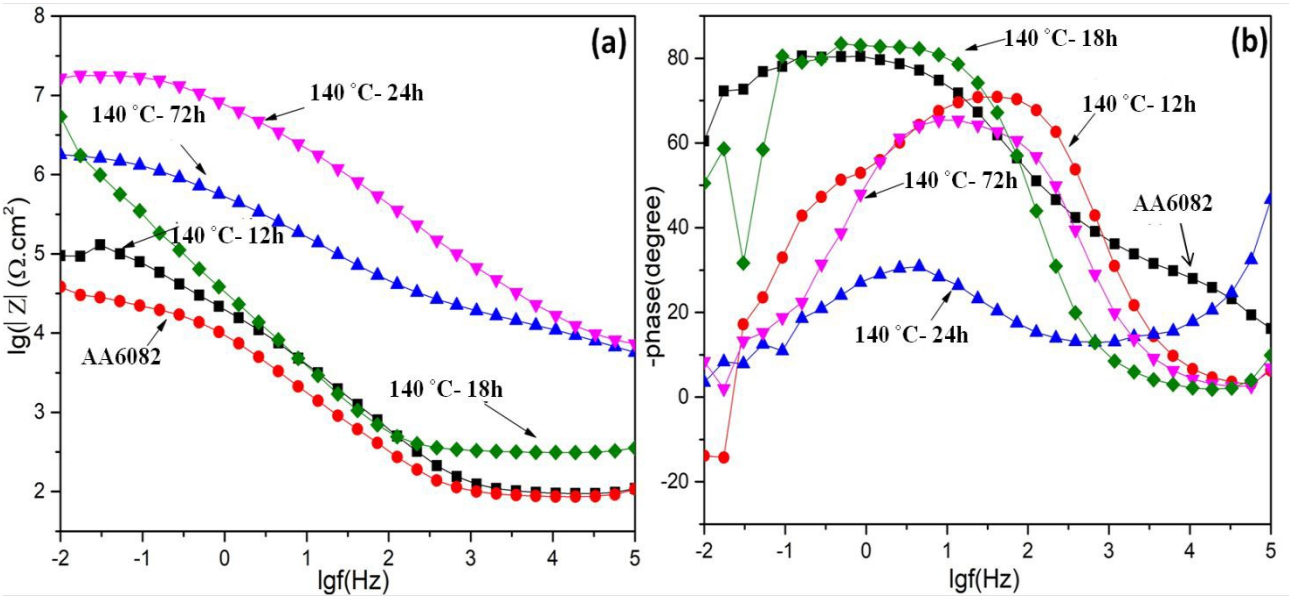

Figure 7(a-b). Impedance and phase plots of CaAl-LDH coated specimens at various synthetic conditions in 0.1 M NaCl solution.

View Article Online
DOI: 10.1039/C9DT01773A

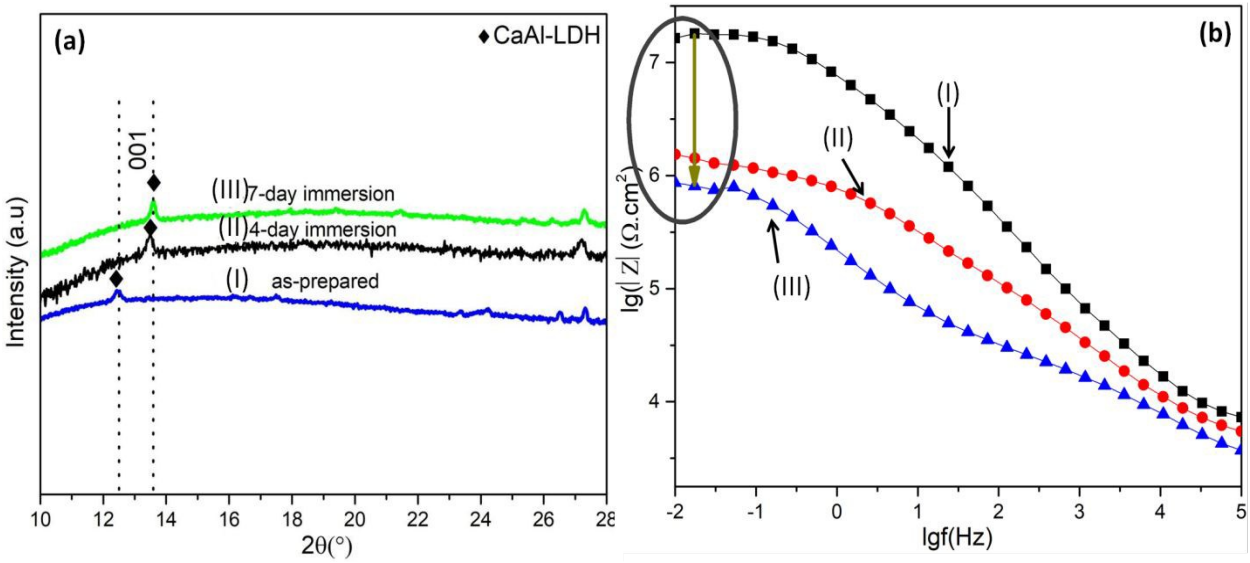

Figure 8. (a) XRD patterns and (b) the corresponding impedance plots of CaAl-LDH synthesized at 140 ˚C-24 h: (I) as-prepared, (II) after 4 days, (III) after 7 days immersion in 0.1 M NaCl solution.

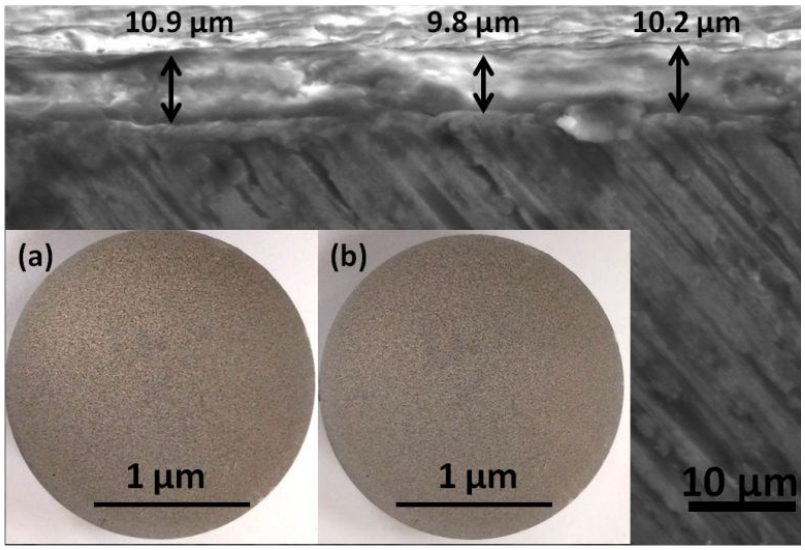

Figure 9. Cross-sectional image of CaAl-LDH after 7 days of immersion in 0.1 M NaCl solution. The insets are digital pictures of the specimen surface: (a) before immersion, (b) after 7 days immersion.

Conclusion

In this contribution, we successfully developed anticorrosive CaAl-LDH thin films on AA6082 substrates by a single step in-situ hydrothermal method. In particular, CaAl-NO_3 LDH uniform vertically alligned structures were formed at 140˚C-24h, which demonstrated excellent corrosion resistance properties with reduction of corrosion current density up to 4 orders of magnitude and impedance of near 3 orders larger at 0.01 Hz compared to bare AA6082 substrate. The

View Article Online
DOI: 10.1039/C9DT01773A

orientation of LDH nano-sheets and morphology (as confirmed by XRD, SEM) are responsible for anion-exchange and the barrier properties at different crystallization times which controlled the corrosion resistance of the CaAl-LDH. The extended reaction times caused more uniform and compact morphologies with small variations in film thickness, which significantly impacted the corrosion current density of CaAl-LDH. It is believed that NO_3^{1-} anions inside the interlayers can further be replaced with various anions (thanks to the anion-exchange behavior of CaAl-LDH) to further improve the anticorrosion behavior of CaAl-LDH thin films.

Conflicts of Interest: The authors declare no conflict of interest.

References

1. J. R. Davis (editor), Corrosion of aluminum and aluminium alloys, ASM International (1999), Ohio, USA.
2. R. Winston Revie, Uhlig's corrosion handbook 3rd edition, John Willey & Sons Inc. (2011) New York, USA.
3. Xhanari, Klodian, and Matjaž Finšgar. "Organic corrosion inhibitors for aluminum and its alloys in chloride and alkaline solutions: a review." *Arabian Journal of Chemistry* (2016).
4. Reye, J. T., McFadden, L. S., Gatica, J. E., & Morales, W. (2004). Conversion Coatings for Aluminum Alloys by Chemical Vapor Deposition Mechanisms.
5. SCHÄFER H, STOCK H R. Improving the corrosion protection of aluminium alloys using reactive magnetron sputtering [J]. Corrosion Science, 2005, 47: 953−964.
6. DIESSELBERG M, STOCK H R, MAYR P. Corrosion protection of magnetron sputtered TiN coatings deposited on high strength aluminium alloys [J]. Surface and Coatings Technology, 2004, 177−178: 399−403
7. Gray, JEl, and Ben Luan. "Protective coatings on magnesium and its alloys—a critical review." *Journal of alloys and compounds* 336.1-2 (2002): 88-113.
8. DALMORO V, DOS SANTOS J H Z, ARMELIN E, ALEM N C,AZAMBUJA D S. A synergistic combination of tetraethylorthosilicate and multiphosphonic acid offers excellent corrosion protection to AA1100 aluminum alloy [J]. Applied Surface Science, 2013, 273:758−768.
9. VOEVODIN N N, KURDZIEL J W, MANTZ R. Corrosion protection for aerospace aluminum alloys by modified selfassembled nanophase particle (MSNAP) sol–gel [J]. Surface and Coatings Technology, 2006, 201: 1080−1084.

View Article Online
DOI: 10.1039/C9DT01773A

10. ARENAS M A, CONDE A, de DAMBORENEA J J. Effect of acid traces on hydrothermal sealing of anodising layers on 2024 aluminium alloy [J]. Electrochimica Acta, 2010, 55: 8704−8708.
11. VENUGOPAL A, PANDA R, MANWATKAR S, SREEKUMAR K,KRISHNA L. RAMA, SUNDARARAJAN G. Effect of micro arc oxidation treatment on localized corrosion behaviour of AA7075 aluminum alloy in 3.5% NaCl solution [J]. Transactions of Nonferrous Metals Society of China, 2012, 22(3): 700−710
12. Iqbal, Muhammad Ahsan, and Michele Fedel. "The effect of the surface morphologies on the corrosion resistance of in situ growth MgAl-LDH based conversion film on AA6082." *Surface and Coatings Technology* 352 (2018): 166-174.
13. Iqbal, Muhammad, and Michele Fedel. "Effect of Synthesis Conditions on the Controlled Growth of MgAl–LDH Corrosion Resistance Film: Structure and Corrosion Resistance Properties." *Coatings* 9.1 (2019): 30.
14. Evans, D. G.; Slade, R. C. T. Structural Aspects of Layered Double Hydroxides. *Struct. Bond.***2006,** *119,* 1-87.
15. Williams, G. R.; O'Hare, D. Towards Understanding, Control and Application of Layered Double Hydroxide Chemistry. *J. Mater. Chem.* **2006,** *16,* 3065-3074.
16. Guo, X. X.; Zhang, F. Z.; Evans, D. G.; Duan, X. Layered Double Hydroxide Films:Synthesis, Properties and Applications. *Chem. Commun.* **2010,** *46,* 5197-5210.
17. Zhou, C. H.; Shen, Z. F.; Liu, L. H.; Liu, S. M. Preparation and Functionality of Clay Containing Films. *J. Mater. Chem.* **2011,** *21,* 15132-15153.
18. J. Tedim, M. L. Zheludkevich, A. N. Salak, A. Lisenkov, M. G. S. Ferreira, *J. Mater. Chem.* **2011**, *21*, 15464.
19. Iqbal, Muhammad Ahsan, and Michele Fedel. "Effect of operating parameters on the structural growth of Zn-Al layered double hydroxide on AA6082 and corresponding corrosion resistance properties. "*Journal of Coatings Technology and Research"* DOI: 10.1007/s11998-019-00227-0. Inpress
20. S. Miyata, Clays Clay Miner., 1983, 31, 305; (b) Y. Isra¨eli G. Taviot-Gu´eho, J.-P. Besse, J.-P. Morel and N. Morel-Fesrosiers, J. Chem. Soc., Dalton Trans., 2000, 791.

View Article Online
DOI: 10.1039/C9DT01773A

21. Israëli, Yaël, et al. "Thermodynamics of anion exchange on a chloride-intercalated zinc–aluminum layered double hydroxide: a microcalorimetric study." *Journal of the Chemical Society, Dalton Transactions* 5 (2000): 791-796.
22. Mishra, Geetanjali, Barsha Dash, and Sony Pandey. "Layered double hydroxides: A brief review from fundamentals to application as evolving biomaterials." *Applied Clay Science*153 (2018): 172-186.
23. Millange, F., Walton, R. I., Lei, L., & O 'Hare, D. (2000). Efficient Separation of Terephthalate and Phthalate Anions by Selective Ion-Exchange Intercalation in the Layered Double Hydroxide Ca2Al (OH) 6⊙ NO3⊙ 2H2O. *Chemistry of Materials*, *12*(7), 1990-1994.
24. Bing, W., Zheng, L., He, S., Rao, D., Xu, M., Zheng, L., ... & Wei, M. (2017). Insights on Active Sites of CaAl-Hydrotalcite as a High-Performance Solid Base Catalyst toward Aldol Condensation. *ACS Catalysis*, *8*(1), 656-664.
25. Taylor, H. F. W. (1973). Crystal structures of some double hydroxide minerals. *Mineralogical Magazine*, *39*(304), 377-389.
26. Rousselot, I., Taviot-Guého, C., Leroux, F., Léone, P., Palvadeau, P., & Besse, J. P. (2002). Insights on the structural chemistry of hydrocalumite and hydrotalcite-like materials: investigation of the series Ca2M3+ (OH) 6Cl· 2H2O (M3+: Al3+, Ga3+, Fe3+, and Sc3+) by X-ray powder diffraction. *Journal of Solid State Chemistry*, *167*(1), 137-144.
27. Renaudin, G., Francois, M., & Evrard, O. (1999). Order and disorder in the lamellar hydrated tetracalcium monocarboaluminate compound. *Cement and Concrete Research*, *29*(1), 63-69.
28. Szabados, M., Mészáros, R., Erdei, S., Kónya, Z., Kukovecz, Á., Sipos, P., & Pálinkó, I. (2016). Ultrasonically-enhanced mechanochemical synthesis of CaAl-layered double hydroxides intercalated by a variety of inorganic anions. *Ultrasonics sonochemistry*, *31*, 409-416.
29. Marappa, Shivanna, S. Radha, and P. Vishnu Kamath. "Nitrate-Intercalated Layered Double Hydroxides–Structure Model, Order, and Disorder." *European Journal of Inorganic Chemistry* 2013.12 (2013): 2122-2128.
30. Panda, H. S., R. Srivastava, and D. Bahadur. "Synthesis and in situ mechanism of nuclei growth of layered double hydroxides." *Bulletin of Materials Science* 34.7 (2011): 1599-1604.

View Article Online
DOI: 10.1039/C9DT01773A

31. Aisawa, Sumio, et al. "Synthesis and thermal decomposition of Mn–Al layered double hydroxides." *Journal of Solid State Chemistry* 167.1 (2002): 152-159.
32. Wu, Qinglan, et al. "Delamination and restacking of a layered double hydroxide with nitrate as counter anion." *Journal of Materials Chemistry* 15.44 (2005): 4695-4700.
33. Kloprogge, J. T. and Frost, R. L., "Fourier transform infrared and Raman spectroscopic study of the local structure of Mg-, Ni-, and Co-hydrotalcites," J. Solid State Chem. **146**, 506–515 (1999).
34. Ni, Z. M., Xia, S. J., Fang, C. P., Wang, L. G., and Hu, J., "Synthesis, characterization and thermal property of Cu/Co/Mg/Al hydrotalcite like compounds," Rare Metal Mater. Eng. **37**, 634–637 (2008).
35. Zhang, Fen, et al. "Corrosion resistance of Mg–Al-LDH coating on magnesium alloy AZ31." *Surface and coatings technology* 258 (2014): 1152-1158.
36. Li, Li, and Nguyen Dang Nam. "Effect of yttrium on corrosion behavior of extruded AZ61 Mg alloy." *Journal of Magnesium and Alloys* 4.1 (2016): 44-51.
37. Jiang, Xiao, Ruiguang Guo, and Shuqin Jiang. "Evaluation of self-healing ability of Ce–V conversion coating on AZ31 magnesium alloy." *Journal of Magnesium and Alloys* 4.3 (2016): 230-241.
38. Wang, Qiang, and Dermot O'Hare. "Recent advances in the synthesis and application of layered double hydroxide (LDH) nanosheets." *Chemical reviews* 112.7 (2012): 4124-4155.